Title
DROPLET MODEL DESCRIPTION OF NUCLEAR MASSES, FISSION BARRIERS AND RADII

Author
Myers, William D.

Publication Date
1974-11-01

Submitted to Nuclear Physics A

LBL-3428 c.2 Repl.
Preprint

6

DROPLET MODEL DESCRIPTION OF NUCLEAR MASSES, FISSION BARRIERS AND RADII

William D. Myers

November 1974

Prepared for the U. S. Energy Research and Development Administration under Contract W-7405-ENG-48

DISCLAIMER

LBL-3428

DROPLET MODEL DESCRIPTION OF NUCLEAR MASSES, FISSION BARRIERS AND RADII[†]

William D. Myers

Lawrence Berkeley Laboratory
University of California
Berkeley, California 94720

November 1974

ABSTRACT

The droplet model of average nuclear properties is briefly explained. This model is then incorporated into an atomic mass formula and the coefficients of the model varied to give the best possible agreement between the calculated and experimental values of masses and fission barriers. The results of the fit are discussed in some detail. The droplet model predictions for nuclear radii are also compared with experiment and found to agree quite well.

[†]Work performed under the auspices of the U.S. Atomic Energy Commission.

1. INTRODUCTION

The droplet model was conceived in order to effect a systematic refinement of the liquid drop model originated by von Weizsacker[1]). Early developments can be found in the works of Bethe[2]), Bohr and Wheeler[3]), Feenberg[4]) and Green[5]). More recent results are contained in the proceedings of the four international conferences on nuclear masses[6-9]), and in the proceedings of two conferences on nuclei far from stability[10,11]). The work that initially stimulated our interest in improving the liquid drop model and some of our preliminary results are contained in refs.[12-16]).

Improved methods for describing average nuclear properties are relevant now because of the recent advances that have been made in our understanding of nuclear masses (and macroscopic properties in general) in terms of a two-part approach. This approach considers nuclear properties, such as masses or density distributions, as being made up of a smooth macroscopic part, and an oscillating microscopic part. Initially the idea of a "two-part approach" was confined to the simple addition of empirical corrections to nuclear mass formulas[17-21]). These corrections were found to be necessary because of fluctuations in the masses due to variations in the nuclear single particle level densities (such as gaps at magic numbers).

Swiatecki[12-14]) developed a method for calculating the shell corrections that is based on a physical model whose main feature is the deviation of the actual nuclear energy level distribution from uniformity. In this approach the relatively minor bunching together of levels that produces gaps at magic numbers gives rise to nuclear mass deviations that correspond closely to those observed. Eventually, a sound physical basis for the two-part approach was provided by the development of Strutinsky's shell

correction method [22]). In this method (see refs. [22-24]) for example) the oscillations observed in nuclear energies and densities are related to the properties of the separate particles of the system which are assumed to be essentially independent and to move in a common nuclear potential.

Progress has also been made in our understanding of the purely macroscopic aspects of nuclear properties, and three items are of special significance for the discussion in the following sections.

The first development of importance has been the clarification of the role of the liquid drop model as an approximate solution of the nuclear many-body problem [25]). For saturating leptodermous† systems like nuclei, we are now aware that the liquid drop model potential energy may be thought of simply as a first order description in terms of two small expansion parameters: the ratio of the surface diffuseness to the size of the system (proportional to $A^{-1/3}$), and the square of the relative neutron excess I^2, where I equals (N-Z)/A.

The second item contributing to our improved understanding of macroscopic properties is the use of the Thomas-Fermi method in self-consistent calculations of nuclear properties. [15]). Such calculations are easily performed and they provide a means of relating many macroscopic properties to their microscopic origin. Of special significance to us here is the fact that the development of the droplet model was supported in a number of ways by Thomas-Fermi calculations like those of Seyler and Blanchard [28]).

---

†leptodermous - having a thin skin. This term has been employed by Tsang, Swiatecki and others [26,27]) for the depiction of distributions that are essentially homogenous except at the surface. Its application implies that all deviations from bulk behavior are confined to a relatively thin surface region.

The third item of importance in our improved understanding of macroscopic properties is the droplet model itself. This model (which is the main subject of the present paper) is a uniform improvement of the liquid drop model that carries the leptodermous expansion to one higher order so as to include mass formula terms in $A^{1/3}$, $I^2A^{2/3}$, and I^4A.

In our earlier work[13,14]) we had fitted a more or less conventional liquid drop model mass formula to the smooth mass surface that results when shell corrections, of the type proposed by Swiatecki [12]), are applied to the experimental masses. Besides the usual liquid drop model terms (which are the volume energy, symmetry energy, surface energy, Coulomb energy and the empirical even-odd mass correction) a surface symmetry energy and Coulomb diffuseness correction were used. Liquid drop model fission barriers were also compared with experiment as a part of the fitting procedure. The inclusion of fission barriers permits more accurate determination of the separate values of the Coulomb and surface energy coefficients, which are highly correlated in a fit to ground state masses alone. We found that the Coulomb energy coefficient (which is inversely proportional to the nuclear radius constant r_o) determined in this way differs by 6 - 10% from that obtained in electron scattering measurements of nuclear sizes [29]). A real discrepancy was seen to exist since both methods were expected to be accurate to one or two percent.

In ref. [15]) we undertook a study to determine whether this discrepancy might not be due to the omission of higher order terms (such as compressibility and surface curvature effects) in the liquid drop model.

Many of these terms had previously been considered one at a time. For example, the surface symmetry term had been considered in refs. [17,19,30]) the compressibility and Coulomb redistribution in refs. [31,32]). Other Coulomb corrections such as the exchange correction [2]) and surface diffuseness correction [17]) had also been used before. The curvature correction to the surface energy was discussed in refs. [33,34]).

The droplet model was developed in the course of our investigation of these higher order terms and some preliminary applications of it have already been made. In ref. [35]) the coefficients that appear in the model were determined by fitting to experimental nuclear masses. The model found other applications in predicting isotope shifts [36]) and in providing a basis for predicting single particle potential well parameters [37]). After the shape dependence of the droplet model had been worked out in ref. [38]) it became possible to investigate the implications of this model for the fission process [39]). A revised version of the droplet model shape dependence is contained in ref. [16]) along with a preliminary set of the adjustable coefficients.

The purpose of the present work is to redetermine these coefficients by fitting to masses, fission barriers, and radii. The predictions of the model are then compared with experiment to give an indication of its range of applicability. One gratifying result of this work is the apparent resolution of the radius constant discrepancy mentioned above. The value of this constant obtained in the droplet model fit no longer differs from that obtained in electron scattering experiments.

2. THE DROPLET MODEL

The droplet model binding energy expression was first derived in ref. [15]). More recently an expanded version of this derivation was given in ref. [16]), where the model was extended to include arbitrary shapes. This latter work should be referred to if the reader desires a more detailed discussion than that given in the brief outline below.

The feature which distinguishes the droplet model from the standard liquid drop model is that the neutron and proton density distributions are allowed to vary so as to minimize the total nuclear energy. This additional freedom leads to the following expression for the binding energy:

$$\begin{aligned} E(N,Z;\text{shape}) = & \left[-a_1 + J\bar{\delta}^2 - \frac{1}{2}K\bar{\varepsilon}^2 + \frac{1}{2}M\bar{\delta}^4\right]A \\ & + \left[a_2 + \frac{9}{4}(J^2/Q)\,\bar{\delta}^2\right]A^{2/3}B_s + a_3A^{1/3}B_k \\ & + c_1Z^2A^{-1/3}B_c - c_2Z^2A^{1/3}B_r - c_3Z^2A^{-1} - c_4Z^{-1/3}Z - c_5Z^2B_w \end{aligned} \tag{1}$$

where

$$\bar{\delta} = \left[I + \frac{3}{16}(c_1/Q)\,ZA^{-2/3}B_v\right] \Big/ \left[1 + \frac{9}{4}(J/Q)A^{-1/3}B_s\right] \tag{2}$$

$$\bar{\varepsilon} = \left[-2a_2A^{-1/3}B_s + L\bar{\delta}^2 + c_1Z^2A^{-4/3}B_c\right] \Big/ K. \tag{3}$$

In these expressions N and Z are the neutron and proton numbers, A is their sum and I is the relative neutron excess (N-Z)/A. The quantity ε is a measure of the average deviation of the bulk density from its nuclear matter value. It is defined by the expression

$$\bar{\varepsilon} = -\frac{1}{3}\left(\frac{\rho - \rho_o}{\rho_o}\right)_{\text{ave.}} \tag{4}$$

To lowest order in $\bar{\epsilon}$ the radius of the nucleus is given by

$$R = r_o A^{1/3}(1 + \bar{\epsilon}) \ , \tag{5}$$

where the nuclear radius constant r_o is related to the equilbrium density ρ_o of infinite nuclear matter by the expression

$$\rho_o = \left(\frac{4}{3} \ \pi r_o^3\right)^{-1} \tag{6}$$

The quantity $\bar{\delta}$ is the value of the local relative neutron excess averaged over the nuclear volume.

$$\bar{\delta} = \left(\frac{\rho_n - \rho_z}{\rho}\right)_{\text{ave}} . \tag{7}$$

Since the effective sharp radii of the neutron and proton distributions can differ, producing a neutron skin of thickness t, the quantity $\bar{\delta}$ is not always equal to I as it is in the liquid drop model. For spherical nuclei these quantitites are related, to first order in t/R, by the expression,

$$\bar{\delta} = I - \frac{3}{2}(t/R). \tag{8}$$

The separate effective sharp radii of the neutron and proton distributions are given by,

$$\begin{aligned} R_N &= R + \frac{Z}{A} t \ , \\ R_Z &= R - \frac{N}{A} t \ , \end{aligned} \tag{9}$$

and this latter quantity is the one to be compared with the results of the electron scattering or μ-mesic atom experiments.

The coefficients appearing in eqs. (1-3) and the values that have been chosen for them are:

a_1 = 15.960 MeV, the volume energy coefficient,

a_2 = 20.69 MeV, the surface energy coefficient,

$$\begin{aligned} J &= 36.8 \text{ MeV}, \quad \text{the symmetry energy coefficient,} \\ r_o &= 1.18 \text{ fm}, \quad \text{the nuclear radius constant,} \end{aligned} \tag{10}$$

and

$$\begin{aligned} a_3 &= 0 \quad \text{Mev}, \quad \text{the curvature correction coefficient,} \\ Q &= 17 \quad \text{MeV}, \quad \text{the effective surface stiffness,} \\ K &= 240 \quad \text{MeV}, \quad \text{the compressibility coefficient,} \\ L &= 100 \quad \text{MeV}, \quad \text{the density-symmetry coefficient,} \\ M &= 0 \quad \text{MeV}, \quad \text{the symmetry anharmonicity coefficient.} \end{aligned} \tag{11}$$

The five Coulomb coefficients that appear are defined in terms of the coefficients above, by the expressions:

$$c_1 = \frac{3}{5}(e^2/r_o) \tag{12}$$
$$= 0.73219 \text{ MeV, the Coulomb energy coefficient,}$$

where $e^2 = 1.4399784$ MeV fm is the square of the electronic charge.

$$c_2 = (c_1^2/336)\,(1/J + 18/K)$$
$$= 0.00016302 \text{ MeV, volume redistribution coefficient,} \tag{13}$$

$$c_3 = \frac{5}{2}\, c_1 (b/r_o)^2$$
$$= 1.28846 \text{ MeV, diffuseness correction coefficient,}$$

where $b = 0.99$ fm is a measure of the diffuseness of the nuclear surface [27]),

$$c_4 = \frac{5}{4}\left(\frac{3}{2\pi}\right)^{2/3} c_1$$
$$= 0.55911 \text{ MeV, exchange correction coefficient,} \tag{14}$$

$$c_5 = \frac{1}{64}\left(c_1^2/Q\right)$$
$$= 0.00049274 \text{ MeV, surface redistribution coefficient.}$$

The quantities B_i, which introduce shape dependence into eqs. (1-3), are discussed in detail in refs. [16,39]). Each of them is concerned with a different aspect of the shape dependence of the binding energy according to the following list:

B_s , the surface energy,

B_c , the Coulomb energy,

B_k , the curvature energy, (15)

B_r , the volume redistribution energy,

B_v , the neutron skin effect,

B_w , the surface redistribution energy .

As usual they are defined so as to have the value unity for a spherical shape.

The three lines of eq. (1) represent the volume, surface and Coulomb contributions to the total binding energy. The four terms in the volume energy contribution (the first line) are: $-a_1$, the binding energy per particle in infinite nuclear matter; $+J\bar{\delta}^2$, the bulk asymmetry term that corrects the binding for the neutron excess; $-\frac{1}{2}K\bar{\epsilon}^2$, the term that gives the extra binding resulting from the competition between various compression and dilitation forces and the bulk compressibility; and, $+\frac{1}{2}M\bar{\delta}^4$, which is a higher order symmetry energy term. The second line consists of two main terms. The first is the surface energy itself, which has the coefficient $\left(a_2 + \frac{9}{4}(J^2/Q)\bar{\delta}^2\right)$. The quantity a_2 is the surface energy coefficient for semi-infinite nuclear matter. The quantity $\frac{9}{4}(J^2/Q)\bar{\delta}^2$ corrects for the fact that some of the excess nucleons are pushed into the surface when $N \neq Z$. The second term in the second line is the curvature correction to the surface energy.

The last line in eq. (1) has five separate parts, all concerning the Coulomb energy. The first is the Coulomb energy of a sharp-surfaced sphere of radius $R = r_o A^{1/3}$. The second term is a correction for the

redistribution of particles in the bulk in response to the Coulomb repulsion which produces a central depression. The third term is a diffuseness correction, the fourth an exchange correction[†], and the last term is a surface redistribution energy associated with the nonuniformity of the neutron skin thickness caused by electrostatic forces.

The other two expressions, eqs. (2) and (3), are used to calculate the equilibrium values of $\bar{\delta}$ and $\bar{\varepsilon}$ for insertion into eq. (1). They are easily understood in terms of a competition between driving and restoring forces. In eq. (3) for example, we see that the average deviation $\bar{\varepsilon}$ of the bulk density from ρ_o is driven by 1) surface squeezing, 2) neutron excess dilatation, and 3) Coulomb dilatation. These driving terms appear, in that order, in the numerator of eq. (3), while the restoring force K appears in the denominator. In eq. (2) we also see that the driving terms I, the overall relative neutron excess, and a Coulomb term that acts to increase the average bulk neutron excess are both in the numerator. The terms in the denominator act as a restoring force which tends to reduce the average bulk asymmetry $\bar{\delta}$.

All of these expressions are more thoroughly explained in ref. [16]).

[†]The usual exchange term is $-c_4 Z^{4/3}/A^{1/3}$, see ref. [2]). Since this is a correction term we have made the simplifying assumption that $Z \approx A/2$. The actual form given in eq. (1) must be used in conjunction with the coefficients, eqs. (10-14), given in the text.

3. MASS FORMULA

The droplet model of macroscopic nuclear properties contains a number of parameters such as the volume energy, surface energy and symmetry energy coefficients. Their values can be determined by varying them until the agreement between experimental and predicted values for nuclear masses, fission barriers and radii is as good as possible. The form of the mass formula employed for this purpose is the following:

$$\begin{aligned}\text{Mass Excess} &= M_N \cdot N + M_H \cdot Z + \text{Droplet Model Term} \\ &+ \text{Shell Correction} + \text{Even-Odd Term} + \text{Wigner Term} \\ &- 0.00001433 \cdot Z^{2.39}\ \text{MeV} \ . \end{aligned} \tag{16}$$

The tabulated masses are atomic rather than nuclear and that is why the last term has been added. It provides a small correction to the data for the binding of the atomic electrons [40]. Another characteristic of the available data is that masses are given as mass excesses relative to ^{12}C as a standard. In this scheme the mass excess of ^{12}C is set to zero, and the true mass of any atom can be obtained from the tabulated mass excess by the relationship [41]:

$$\text{True Mass} = \text{Mass Excess} + 931.504 \cdot A\ \text{MeV} \tag{17}$$

In this system the coefficients of the first two terms in eq. (16), which are the mass excesses of the neutron and the hydrogen atom, have the values [41]:

$$\begin{aligned} M_N &= 8.07169\ \text{MeV}, \\ M_H &= 7.28922\ \text{MeV}. \end{aligned} \tag{18}$$

3.1 Shell Corrections

The shell corrections employed were the same as in our original work [12,13]), with the slight modification in shape dependence added in ref. [14]). These references discuss the physical motivation behind the expressions which are reproduced here.

For spherical nuclei the shell correction is taken to be

$$S(N,Z) = C\cdot\left[\frac{F(N) + F(Z)}{\left(\frac{1}{2}A\right)^{2/3}} - cA^{1/3}\right] \tag{19}$$

where

$$F(N) = q_i(N - M_{i-1}) - \frac{3}{5}\left(N^{5/3} - M_{i-1}^{5/3}\right) , \tag{20}$$

for $M_{i-1} < N < M_i$, and both C and c are adjustable coefficients. The quantities q_i are defined by

$$q_i(n) = \frac{3}{5}\cdot\frac{M_i^{5/3} - M_{i-1}^{5/3}}{M_i - M_{i-1}} , \tag{21}$$

and the quantities M_i (the magic numbers) are chosen to have the values 2, 8, 14, 28, 50, 82, 126 and 184.

As before, the damping of shell effects with deformation is taken to have the relatively simple functional form,

$$(1 - 2\theta^2)\, e^{-\theta^2} , \tag{22}$$

where θ, as it is used here and in ref. [13,14]), is a measure of the deviation of the nuclear shape from spherical. For small distortions described by the Legendre polynomial P_2 according to the expression

$$R(\mu) = R[1 + \alpha P_2(\mu)] \quad , \tag{23}$$

the quantity θ is given by

$$\theta = \alpha/\alpha_o \tag{24}$$

where

$$\alpha_o = \sqrt{5}\ (a/r_o)A^{-1/3} \quad . \tag{25}$$

The quantity a that appears in eq. (25) is an adjustable coefficient that determines how quickly the shell effects damp out as the shape is changed.

Since only the droplet model and shell effect terms in eq. (16) are shape dependent, the whole expression can be recast (using the expressions for the shape dependences B_i given in Section V of ref. [16]) in the form

$$M = M_o + E\theta^2 + F\theta^3 + S \cdot (1 + 2\theta^2)e^{-\theta^2} \tag{26}$$

If the lowest minimum in this function is other than spherical then the nucleus is predicted to be deformed in its ground state. The resulting quadrupole moment is given by the expression

$$Q_o = 6/5 \cdot (r_o A^{1/3})^2 Z\alpha \quad (1 + \alpha/4 + \alpha^2/2 \ldots.)\text{fm}^2 \tag{27}$$

As in previous work, the quantity we refer to here as the Shell Correction is the difference between M_o and the minimum energy in eq. (26). For the three adjustable parameters that appear in the shell correction we have chosen to retain the values used earlier [14],

$$C = 5.8 \text{ MeV} ,$$
$$c = 0.325 , \qquad (28)$$
$$a/r_o = 0.444 .$$

In the actual fit, an entirely empirical function F(N or Z) similar to the one given in section 7.3 of ref. [13]) was employed for N, Z < 20. This function was determined from N = Z nuclei with the aid of eq. (19) after subtracting the other terms of eq. (16)

3.2 The Even-Odd Term

In our previous work [13,14]) an even-odd mass term was employed that had the value $+11/\sqrt{A}$, 0, $-11/\sqrt{A}$ depending on whether the nucleus was odd, odd-A, or even. Here we use a slightly different version that allows for the fact that the separation between the odd and odd-A mass surfaces is slightly smaller than the separation between the even and odd-A surfaces (see the caption to fig. 2-5 in ref. [42]), for example). Figure 1 shows how the correction was made so the mean mass surface continues to pass through the masses halfway between the even and the odd nuclei. In this scheme the correction is $(\Delta - \frac{1}{2}\delta)$, $(+\frac{1}{2}\delta)$, $(-\Delta + \frac{1}{2}\delta)$ depending on whether the nucleus is odd, odd-A, or even, where $\Delta = 12/\sqrt{A}$ and $\delta = 20/A$.

3.3 The "Wigner Term"

There is a vee-shaped trough in the nuclear mass surface (see ref. [13]) section 7.2, for example) that is not a shell-effect in the usual

sense. Nor is it an even-odd effect of the type mentioned in the previous section. A term of this kind in the mass equation, proportional to $|I|$, was first discussed by Wigner, see ref. [43]) and references there to the original works, or ref. [44]) Section III.

A relatively simple argument serves to show how such a term can arise from the increased overlap of the wavefunctions of particles in identical orbits. Because of saturation the interaction between two particles in the nucleus is proportional to 1/A. If the particles in identical orbits interact somewhat more strongly than the average, this contribution to the total energy can be obtained by multiplying $-\varepsilon C/A$ times the number of identical pairs. (Here $-C/A$ is the average interaction and ε is a measure of the enhancement due to the particles being in the same orbit.) Figure 2 explains how the identical pairs are counted. The considerations there lead us to write,

$$\left(\begin{array}{c}\text{Number of}\\ \text{identical pairs}\end{array}\right) = \frac{3}{2}A - |N-Z| - \begin{cases} 0\ , \text{ for even} \\ \frac{1}{2}\ , \text{ for odd } A \\ 1\ , \text{ for odd} \end{cases} - \begin{cases} 1, \text{ for } N=Z \text{ odd} \\ 0, \text{ for all other} \end{cases} \tag{29}$$

The total amount of additional energy contributed by these bonds can then be written

$$W\left[-\frac{3}{2} + |I| + \delta + \Delta\right] \tag{30}$$

where

$$\delta = 1/A \cdot \begin{cases} 0\ , \text{ for even} \\ \frac{1}{2}\ , \text{ for odd-A} \\ 1\ , \text{ for odd} \end{cases} \tag{31}$$

$$\Delta = 1/A \cdot \begin{cases} 1\ , \text{ for } N=Z \text{ odd} \\ 0\ , \text{ for all other} \end{cases} \tag{32}$$

and W, which replaces εC, is to be determined by fitting to nuclear masses.

The first term in the bracket is a constant. Such terms (of order A^0) can arise from many sources. We will not retain this particular contribution in order to be consistent with the general formulation of the droplet model where the highest order term is $A^{1/3}$. The second term, showing the $|I|$ dependence, is the one we originally sought. The third term will not be retained since it is an even-odd correction of the type discussed in the previous section, and its contribution to the nuclear mass is included in the empirical term described there. The last term applies only to $N = Z =$ odd nuclei but we will keep it because it is clearly called for by the experimental masses (see ref. [44]), Table I). The form adopted for our "Wigner term" is

$$E_{Wigner} = W(|I| + \Delta) \quad , \tag{33}$$

and choosing 30 MeV for the value of W gives good agreement with experiment.

On the basis of the derivation given above the size of the "Wigner Term" contribution to the total energy appears to be independent of shape. However, at scission into two parts the term jumps to twice its original value. In an extreme idealization the shape dependence of this term (and the even-odd term and some terms of order A^0) is a discontinuous step function. In practice the step is washed out since particles find it more and more difficult to explore the whole nuclear volume when the neck formed between nascent fragments closes off as the system moves toward scission. In general such a shape dependence, confined to the vicinity

of scission, may be expected to lead to (attractive or repulsive) "contact potentials" between fission fragments (or colliding heavy-ions).

4. COMPARISON WITH EXPERIMENT

The primary data employed for the determination of the droplet model coefficients were the 1698 experimental atomic masses with $A \geqslant 10$ taken from the 1971 compilation of Wapstra and Gove [41]). These were supplemented by 62 experimental fission barriers, 109 ground state deformations and 6 nuclear charge radii. The actual fit was weighted 3/4 to the masses and 1/4 to the fission barriers.† If we had given each datum equal weight the large number of masses would have dominated leaving the barriers with little influence on the results. The radii were only used in the fitting procedure when we had to choose between $r_0 = 1.17$ and 1.18 fm in rounding off the final set of coefficients. The deformations are determined largely by the coefficients in the shell effect function whose values were taken from our previous work [14]). The resulting droplet model predictions for all of these quantities are discussed in the following sections.

4.1 Beta-Stability Properties

In order to appreciate the quality of the fit let us compare the general features of the experimental mass surface with those predicted by the theory. One way of doing this is to recognize that the mass surface is essentially a steep-sided valley whose main axis bends away from the $N = Z$ line toward neutron rich nuclei and whose cross-section is approximately parabolic.

The solid curves in fig. 3 show how the valley of beta-stability is expected to vary as a function of the mass number A. The character-

†A minor error was found in the barrier calculations after the fitting was completed. Its correction resulted in slightly improved agreement with experiment.

istics of parabolas fitted (at constant A) to the mass surface are given in this figure for comparison with the corresponding experimental values given by points. The quantity V_A is the minimum value of the parabola, Y_A is the value of the neutron excess (Y = N-Z) at the minimum, and C_A is the curvature of the parabola. One sees that the lowest point on the mass surface is at A ≈ 115, that the displacement of the valley away from the N = Z line increases steadily, and the curvature of the bottom of the valley decreases with increasing A. One also sees that the agreement between theory and experiment is so good that we must display the difference (as is done in fig. 4) in order to see the remaining discrepancies.

Figure 4 shows that the minimum values of the parabolas fitted to the experimental masses generally lie below those predicted, and that the curvature of the experimental parabolas is generally greater than that predicted. These two deviations tend to compensate. In addition note the relatively large excursion of the experimental values of V_A away from those predicted in the vicinity of A = 190. This difference seems to be due to the relatively poor quality of our shell corrections for nuclei at the end of the rare-earth region. Another deviation that is probably due to shell effects is the tendency of the experimental valley of beta-stability to straighten out in the actinide region and not continue to bend away from the N = Z line as is predicted by the model. This tendency shows up as a downward deviation of Y_A in fig. 4b for A ≥ 210. In our efforts to understand this deviation we tried other sets of shell corrections [45-47] which reduced the discrepancy to varying degrees but none of them eliminated it entirely. We also found that by choosing what appear to be unphysical values for the droplet model coefficients L and M, which are concerned

with higher order asymmetry effects, we could straighten out the valley of beta-stability in the actinide region. This had the effect of reducing the discrepancy at the cost of distorting the whole fitting procedure so as to give values that we felt were unreasonable for many of the coefficients. To avoid this undesirable tendency the coefficients L and M were fixed at nominal values chosen ahead of time and not allowed free variation in the fit. The compressibility coefficient K was also fixed at a nominal value close to the one that gave the best agreement with experiment.

4.2 Final Mass Differences

Another way of displaying the differences between the experimental masses and the theoretical predictions is to plot the individual mass differences versus the neutron number as is done in fig. 5. This plot, which should be compared with similar ones in our previous work[14]), shows once again how poor our shell correction function is at the end of the rare earth region. The agreement between our shell function and the experimental one is also poor for the heavy elements. Microscopic methods for calculating shell effects such as the Strutinsky procedure[22-24]) were expected to give a better account of these features but their overall agreement with experiment (as can be seen in figs. 6 and 7) is about the same.

Of course, it is possible some of the deviations seen in figs. 3-7 are due to as yet unrecognized macroscopic effects rather than being completely due to shell effects. Another way of displaying the residual errors that might be useful for identifying such trends is a contour plot like fig. 8. Here the same data as are shown in fig. 5 are given as contours in the N,Z plane. The main feature of this diagram seems to be

the hole near N = 110, Z = 75 due to over-correction for the shell effects in this region.

4.3 Fission Barriers

As was mentioned earlier, the droplet model coefficients were adjusted to give the best possible agreement between theory and experiment for both ground state masses and fission barriers. In the previous section we saw that the residual errors in the ground state masses seemed to be due to insufficiently precise shell corrections. There was no indication that improvements were needed in the macroscopic part of the theory. However, a comparison between calculated and experimental fission barriers shows that systematic deviations remain that may be due to some shortcoming of the droplet model.

In fig. 9a (based on the data from Table 1) the experimental fission barriers have been plotted relative to the ground state mass according to the scheme shown in fig. 10. The droplet model saddle masses for the same nuclei are shown in fig. 9b and the residual error in fig. 9c. The calculated values are seen to differ from the experimental ones in a systematic (almost linear) way as one moves through the periodic table. If we had included shell corrections at the saddle point our calculated values would have agreed better in the actinide region but would not have changed much for the lighter nuclei. Negative values of the curvature correction coefficient, and a modified type of surface energy function[48]) were both found effective in reducing the differences in saddle masses but they made the fit to ground state masses worse. So far no satisfactory explanation for these deviations has been found.

4.4 Deformations

As in our previous work[13,14]) one of the results of the calculation of shell effects is a prediction of nuclear ground state deformations. During the fitting procedure the calculated values were compared with the experimental ones from ref. [49]). Fig. 11 shows that there is rough agreement between theory and experiment for nuclei in the rare-earth and actinide regions. The main deviations seem to be associated (as with the mass deviations) with the inability of our shell correction function to adequately portray the behavior of nuclei at the upper end of the rare-earth region.

4.5 Radii

The droplet model parameters chosen to give the best fit for masses and fission barriers also lead to predictions of nuclear charge radii in quite good agreement with experiment. The droplet model fit seems to have resolved the discrepancy, mentioned earlier[13,14]), that existed between the nuclear radius constant inferred from a liquid drop model fit to masses, and that obtained from electron scattering measurements of nuclear charge radii. Table 2 lists the calculated and experimental radii that are compared in fig. 12. This figure also shows how the effective sharp radii of the neutron and proton distributions are expected to vary for nuclei along beta-stability and how these radii are related to the radius constant r_o.

5. REMARKS

The development of the droplet model was originally undertaken to improve the liquid drop model approach by carrying the leptodermous expansion of nuclear properties to one higher order in $A^{1/3}$. We hoped, in this way, to help fill the gap existing between the usual liquid drop model (terms of order A and $A^{2/3}$) and the various terms of non-statistical origin such as shell effects, even-odd effects, Wigner term, etc. This work is brought to completion here with the determination of values for the various coefficients that enter and the comparison of calculated and experimental values for masses, fission barriers and radii.

The differences that remain when the droplet model is used to calculate ground state masses seem to be due to inadequate shell corrections, but this is not the case for fission barriers. For barriers, the differences vary smoothly as one moves up the periodic table indicating that some effect of a statistical nature may still be missing.

Some of the coefficients we have evaluated here (the volume energy coefficient, symmetry energy coefficient, surface energy coefficient, and nuclear radius constant, for example) may be considered constants of nature. These constants are probably more accurately determined from the experimental data when the droplet model is used than was possible with the liquid drop model. When the droplet model is used there is less need for these coefficients to assume slightly incorrect values to compensate for missing higher order terms. The droplet model also provides a more accurate way for extrapolating far from beta-stability because of the higher order effects that are included. Since a number of higher order shape dependencies (such as the shape dependence of the Coulomb redistri-

bution energy or surface symmetry energy) are included, the droplet model will be important in calculations of heavy-ion collisions where highly distorted shapes are involved.

These gains in understanding and completeness are provided by the droplet model at the cost of a substantial increase in the complexity of the treatment. However, the widespread availability of high-speed electronic computers makes this increased complexity tolerable for many applications. In addition the author is preparing a table that will contain the droplet model values for the masses, fission barriers, deformations, radii, etc. for all nuclei that are predicted to be particle stable. Copies of this table will be available to interested users.

ACKNOWLEDGMENTS

The entire droplet model approach was conceived and carried out in collaboration with W. J. Swiatecki whose influence is to be seen in every part of the work. The author has also, in the years over which this work was brought to completion, benefitted substantially from discussions with E. R. Hilf, J. R. Nix, P. A. Seeger, and C. F. Tsang. Important contributions were made by H. von Groote, R. W. Hasse, P. Möller, S. G. Nilsson and D. Sprung with considerable programming assistance provided by Tom Strong.

REFERENCES

1. C. F. Weizsacker, Zeit. Physik 96 (1935) 431
2. H. A. Bethe and R. F. Bacher, Rev. Mod. Phys. 8 (1936) 82
3. N. Bohr and J. A. Wheeler, Phys. Rev. 56 (1939) 426
4. E. Feenberg, Rev. Mod. Phys. 19 (1947) 239
5. A. E. S. Green, Phys. Rev. 95 (1954) 1006
6. Proc. of the Int. Conf. on Nuclidic Masses, H. E. Duckworth (ed.), Univ. of Toronto Press, Toronto (1960)
7. Nuclidic Masses, Proc. of the Second Int. Conf. on Nuclidic Masses, W. H. Johnson, Jr., (ed.), Springer-Verlag, Wein-New York (1964)
8. Proc. of the Third Int. Conf. on Atomic Masses, R. C. Barber (ed.), Univ. of Manitoba Press, Winnipeg (1968)
9. Atomic Masses and Fundamental Constants 4, Proc. of the Fourth Int. Conf. on Atomic Masses, J. H. Sanders and A. H. Wapstra (eds.), Plenum Press, London-New York (1972)
10. Nuclides far off the Stability Line, Proc. of the Lysekil Symposium (1966), Arkiv Fysik 36 (1967) 343-52
11. Proc. Int. Conf. on the Properties of Nuclei far from the Region of Beta-Stability, Leysin, Switzerland, CERN 70-30 (1970)
12. W. J. Swiatecki, Proc. Conf. on Nuclidic Masses, Vienna, 1963, ed. by W. H. Johnson, Jr. (Springer-Verlag, Wein-New York, 1964) p. 58
13. W. D. Myers and W. J. Swiatecki, Nucl. Phys. 81 (1966) 1-60
14. W. D. Myers and W. J. Swiatecki, Nuclides Far off the Stability Line, Proc. of the Lysekil Symposium, 1966, Arkiv Fysik 36 (1967) 343-352
15. W. D. Myers and W. J. Swiatecki, Ann. Phys. (N.Y.) 55 (1969) 395-505
16. W. D. Myers and W. J. Swiatecki, Ann. Phys. (N.Y.) 84 (1974) 186-210
17. A. G. W. Cameron, Can. J. Phys. 35 (1957) 1021-32
18. F. S. Mozer, Phys. Rev. 116 (1959) 970
19. P. A. Seeger, Nucl. Phys. 25 (1961) 1-135
20. N. Zeldes, M. Gronau and A. Lev, Nucl. Phys. 63 (1965) 1-75
21. N. Zeldes, A. Grill and A. Simievic, Mat. Fys. Skr. Dan. Vid. Selsk. 3, No. 5 (1967)
22. M. Brack, et al., Rev. Mod. Phys. 44 (1972) 320
23. J. R. Nix, Ann. Rev. Nucl. Sci. 22 (1972) 65

24. S. G. Nilsson, et al., Nucl. Phys. A131 (1969) 1
25. W. D. Myers; in "Dynamic Structure of Nuclear States", Proceedings of the 1971 Mont Tremblant International Summer School, Univ. of Toronto Press (1972)
26. C. F. Tsang, Ph. D. Thesis, Lawrence Radiation Laboratory Report UCRL - 18899 (1969)
27. W. D. Myers, Nucl. Phys. A204 (1973) 465-484
28. R. G. Seyler and C. H. Blanchard, Phys. Rev. 124 (1961) 227
29. H. R. Collard, L. R. B. Elton and R. Hofstadter, in "Nuclear Radii", Vol. 2, group I Landolt-Börnstein, Numerical data and functional relationships in science and technology. (Springer-Verlag, Berlin, 1967)
30. E. Feenberg, Rev. Mod. Phys. 19 (1947) 239
31. W. J. Swiatecki, Proc. Phys. Soc. London A63 (1950) 1208
32. W. J. Swiatecki, Phys. Rev. 83 (1951) 178
33. E. Hilf and G. Süssmann, Phys. Letters 21 (1966) 654
34. H. von Groote and E. Hilf, Nucl. Phys. A129 (1969) 513
35. S. Ludwig, et al., Nucl. Phys. A203 (1973) 627-40
36. W. D. Myers, Phys. Letters 30B (1969) 451-4
37. W. D. Myers, Nucl. Phys. A145 (1970) 387-400
38. W. D. Myers, and W. J. Swiatecki, Lawrence Radiation Laboratory, UCRL-19543 (1970)
39. R. W. Hasse, Ann. Phys. 68 (1971) 377-461
40. L. L. Foldy, Phys. Rev. 83 (1951) 397
41. A. H. Wapstra and N. B. Gove, Nuclear Data Tables 9 (1971) 265
42. A. Bohr and B. R. Mottelson, Nuclear Structure, Vol. I, (W. A. Benjamin, Inc., New York, 1969)
43. J. M. Blatt and V. F. Weisskopf, Theoretical Nuclear Physics, (John Wiley and Sons, New York, 1952)
44. G. T. Garvey, et al., Rev. Mod. Phys. 41 (1969) 51-580
45. P. Möller, private communication
46. P. A. Seeger, private communication
47. J. R. Nix, private communication
48. H. J. Krappe and J. R. Nix, Proc. Third Int. Conf. on Physics and Chemistry of Fission, (IAEA, Vienna, 1974) paper IAEA-SM-174/12

49. K. E. G. Löbner, M. Vetter and V. Hönig, Nucl. Data A7 (1970) 495-564.

50. M. Yamada, Prog. Theor. Phys. 32 (1964) 512.

51. T. Kodama, Prog. Theor. Phys. 45 (1971) 1112-1122.

Table 1. Experimental Fission Barriers and Saddle Masses

Name	Z	A	Experimental Barrier	Relative Saddle Mass			
				Experimental	Calculated	Difference	
Lu	71	173	28.0	27.2	30.9	-3.7	a)
Ta	73	179	26.1	25.0	27.9	-2.9	a)
Re	75	185	24.0	22.0	24.8	-2.8	a)
Os	76	186	23.4	21.4	23.3	-1.9	a)
		187	22.7	20.5	23.2	-2.7	a)
		188	24.2	21.8	23.2	-1.4	a)
Ir	77	189	22.6	20.2	21.6	-1.4	a)
		191	23.7	20.7	21.5	-0.8	a)
Tl	81	201	22.3	13.8	15.2	-1.4	a)
Bi	83	207	21.9	11.1	12.2	-1.1	a)
		209	23.3	11.1	12.0	-0.9	a)
Po	84	210	21.0 b)	10.1	10.9	-0.8	a)
		211	19.7	10.0	10.8	-0.8	a)
		212	19.5	10.9	10.7	0.2	a)
At	85	213	17.0	9.6	9.8	-0.2	a)
Rn	86	216	13.5	8.4	8.6	-0.2	c)
Ra	88	225	9.0	8.2	6.6	1.6	d)
		227	8.0	8.0	6.4	1.6	d)
Ac	89	226	8.0	7.0	6.0	1.0	d)
		227	7.3	6.6	5.9	0.7	d)
		228	7.2	6.8	5.8	1.0	d)
Th	90	230	6.5	5.8	5.2	0.6	e)
		232	6.2	5.7	5.0	0.7	e)
		234	6.5	6.3	4.8	1.5	e)
Pa	91	231	5.9	4.9	4.7	0.2	f)
		232	6.1	4.9	4.6	0.3	f)
		233	6.0	5.0	4.5	0.5	f)
U	92	232	5.5	4.0	4.2	-0.2	e)
		234	6.2	4.6	4.0	0.6	e)

(Continued)

Table 1 (Continued)

		235	6.1	4.5	4.0	0.5	f)
		236	5.7	4.3	3.9	0.4	e)
		237	6.4	5.0	3.8	1.2	f)
		238	5.9	4.9	3.8	1.1	e)
		239	6.6	5.6	3.7	1.9	f)
		240	6.0	5.4	3.6	1.8	e)
Np	93	234	5.4	3.3	3.7	-0.4	f)
		235	5.6	3.6	3.6	0.0	f)
		236	5.7	3.6	3.6	0.0	f)
		237	5.7	3.9	3.5	0.4	f)
		238	6.0	4.0	3.4	0.6	f)
		239	5.9	4.3	3.4	0.9	f)
Pu	94	238	5.9	3.6	3.1	0.5	e)
		239	6.4	3.9	3.1	0.8	f)
		240	5.8	3.6	3.0	0.6	e)
		241	6.3	4.1	3.0	1.1	f)
		242	5.6	3.8	2.9	0.9	e)
		243	6.1	4.3	2.9	1.4	f)
		245	5.7	4.3	2.7	1.6	f)
Am	95	240	6.4	3.4	2.7	0.7	f)
		241	6.0	3.3	2.7	0.6	f)
		242	6.4	3.7	2.6	1.1	f)
		243	6.0	3.7	2.6	1.1	f)
		244	6.2	3.8	2.5	1.3	f)
		245	5.9	4.0	2.5	1.5	f)
		247	5.6	4.1	2.4	1.7	f)
Cm	96	244	6.1	3.2	2.3	0.9	e)
		245	6.4	3.4	2.2	1.2	f)
		247	6.2	3.5	2.1	1.4	f)
		248	6.2	3.9	2.1	1.8	e)

(Continued)

Table 1 (Continued)

		249	5.8	3.7	2.0	1.7 [f]
		250	5.2	3.6	2.0	1.6 [e]
Bk	97	249	6.1	3.2	1.8	1.4 [f]

Footnotes to Table 1.

a) L.G. Moretto, et al., Phys. Letters 38B (1972) 471

b) Average of two values given.

c) H. Freisleben, H.C. Britt and J.R. Huizenga, Proceedings of the Third International Conference on the Physics and Chemistry of Fission, paper IAEA/SM - 174/81

d) Inferred from figures in E. Konecny, H.J. Specht and J. Weber, ibid., paper IAEA/SM - 174/20

e) B.B. Back, et al., ibid., paper IAEA/SM - 174/27.

f) B.B. Back, et al., ibid., paper IAEA/SM - 174/201

Table 2. Calculated and Experimental Nuclear Charge Radii[a])

Nucleus	Experiment[b])	Distribution Parameters[c]) c	a	w	$R_Z/A^{1/3}$ Experimental[d])		Calculated[e])
^{40}Ca	e	3.650	0.517	0	1.138	1.152	1.133
	e	3.676	0.585	-0.102	1.154		
	e,μ	3.697	0.587	-0.083	1.163		
	e	3.669	0.584	-0.102	1.152		
^{48}Ca	e	e.650	0.498	0	1.066	1.091	1.094
	e	3.744	0.526	-0.03	1.095		
	e,μ	3.797	0.534	-0.048	1.109		
	e	3.737	0.525	-0.03	1.093		
^{120}Sn	e	5.315	0.575	0	1.119	1.132	1.124
	μ	5.495	0.507	0	1.145		
^{138}Ba	μ	5.771	0.496	0	1.144	1.145	1.123
	e	5.83	0.407	0	1.146		
^{142}Nd	e	5.614	0.587	0.096	1.118		1.133

^{208}Pb	μ	6.712	0.481	0	1.152		
	μ	6.659	0.514	0	1.146		
	μ	6.720	0.504	-0.061	1.154		
	e	6.47	0.523	0	1.115		
	e	6.38	0.537	0.130	1.105	1.134	1.133
	e	6.40	0.542	0.140	1.109		
	e	6.66	0.503	0	1.145		
	e	6.597	0.550	0	1.139		
	e	6.628	0.544	-0.062	1.142		

Footnotes to Table 2.

a) Experimental data from table 3 of R. C. Barrett, Rep. Prog. Phys. 37 (1974) 1-54.

b) The symbol e is used for electron scattering and μ for μ-mesic atom experiments.

c) The charge densities were parameterized according to the expression

$$\rho_z = \rho_c \left[1 + w(r/c)^2\right] \Big/ \left\{1 + \exp[(r-c)/a]\right\}$$

d) The experimental value of the effective sharp radius of the charge distribution can be calculated with the expression

$$R_Z = c\left[1 + \frac{(1+2w)}{(1+w)} \cdot \frac{\pi^2}{3} \cdot (a/c)^2 + \ldots.\right] \text{, see ref. } ^{15}).$$

e) Eqs. 2, 3, 5, 8 and 9 are used to calculate the droplet model value of R_Z.

FIGURE CAPTIONS

Fig. 1. Scheme used for the even-odd correction.

Fig. 2. Origin of the "Wigner term" in terms of increased binding for nucleons in identical orbits.

Fig. 3. Experimental and calculated properties of the valley of beta-stability are plotted against mass number A. The points shown (for every fifth A value) were determined by fitting the quadratic function $M_A = V_A + \frac{1}{2} C_A(Y - Y_A)^2$ to isobaric sequences after first correcting the experimental masses for shell effects, the even-odd mass differences, the Wigner term and the binding of the atomic electrons. The solid lines represent the droplet model predictions for these same quantities.

Fig. 4. The difference between the experimental and calculated values of V_A, Y_A and C_A from fig. 3 are plotted against mass number A in order to display the remaining deviations. This particularly useful way of displaying the data was inspired by the work of Yamada[50]), Kodama[51]) and Ludwig et al.[35])

Fig. 5. The experimental and calculated shell effects and their differences are shown as functions of the neutron number. Isotopes of an element are connected by a line. The large negative deviations at the beginning of the periodic table are for nuclei outside of the fit region, which began at A = 10. A small histogram to the right of part (c) shows how the final errors are distributed for nuclei in the fit region. The substantial weight given to fitting fission barriers is presumably responsible for pulling the error distribution slightly to one side so that the mass residuals are not equally distributed about zero.

Fig. 6. This figure is like fig. 5 for N and Z < 20 where an empirical shell function is used. The remainder of the calculated shell effects are from Seeger[46]) who used the Strutinsky method. The droplet model coefficients were redetermined to obtain the best agreement with masses and fission barriers. Their values changed very little and the quality of the fit was about the same.

Fig. 7. This figure employs an empirical shell function for N and Z < 20 as in figs. 5b and 6b. It uses the shell corrections provided by Seeger (see fig. 6b) up to the middle of the rare earth region then switches to a set of corrections provided by Möller[45]). This latter set of corrections was adjusted to the heavy element region where it agrees quite well with experiment. Even though the droplet model coefficients were also redetermined, the overall agreement is about the same as that shown in figs. 5 and 6.

Fig. 8. The differences that remain between the experimental masses and those calculated with eq. (16) after the droplet model coefficients have been adjusted to give the best overall agreement for masses and fission barriers.

Fig. 9. Experimental and calculated saddle masses and their differences are plotted against neutron number N for nuclei listed in Table 1. The relationship between the experimental ground state shell correction, fission barrier and saddle mass can be seen in fig. 10.

Fig. 10. Schematic diagram to show how the calculated fission barrier is related to the calculated saddle mass and the ground state shell correction. The figure also shows how shell effects can cause the experimental barriers to be slightly higher.

Fig. 11. Calculated and experimental quadrupole moments for nuclei in the rare-earth and actinide region are plotted against neutron number. The moments plotted are for those even-even nuclei listed in ref. [49]) with the omission of a few points with large errors whose tabulated values differed substantially from those of adjacent nuclei.

Fig. 12. Various quantities characteristic of the radial extent of spherical nuclei are plotted versus the mass number A. The dashed lines labeled N and Z correspond to the droplet model predictions for the quantities $(R_N/A^{1/3})$ and $R_Z/A^{1/3})$ for nuclei along the bottom of the valley of beta-stability. The solid line, which is the weighted mean of the neutron and proton lines, represents the value of $(R/A^{1/3})$ for the total nucleon density. The solid dots correspond to the experimental values of $(R_Z/A^{1/3})$ for various spherical nuclei given in table 2. The error bars of ± .012 fm were chosen to represent the spread in values observed in the tabulated results. Solid triangles indicate the droplet model value of $(R_Z/A^{1/3})$ for these same nuclei. For comparison a dot-dashed line is drawn across the figure at 1.18 fm which is the value of r_o (the constant related to ρ_o by eq. (6)) determined by the fitting procedure.

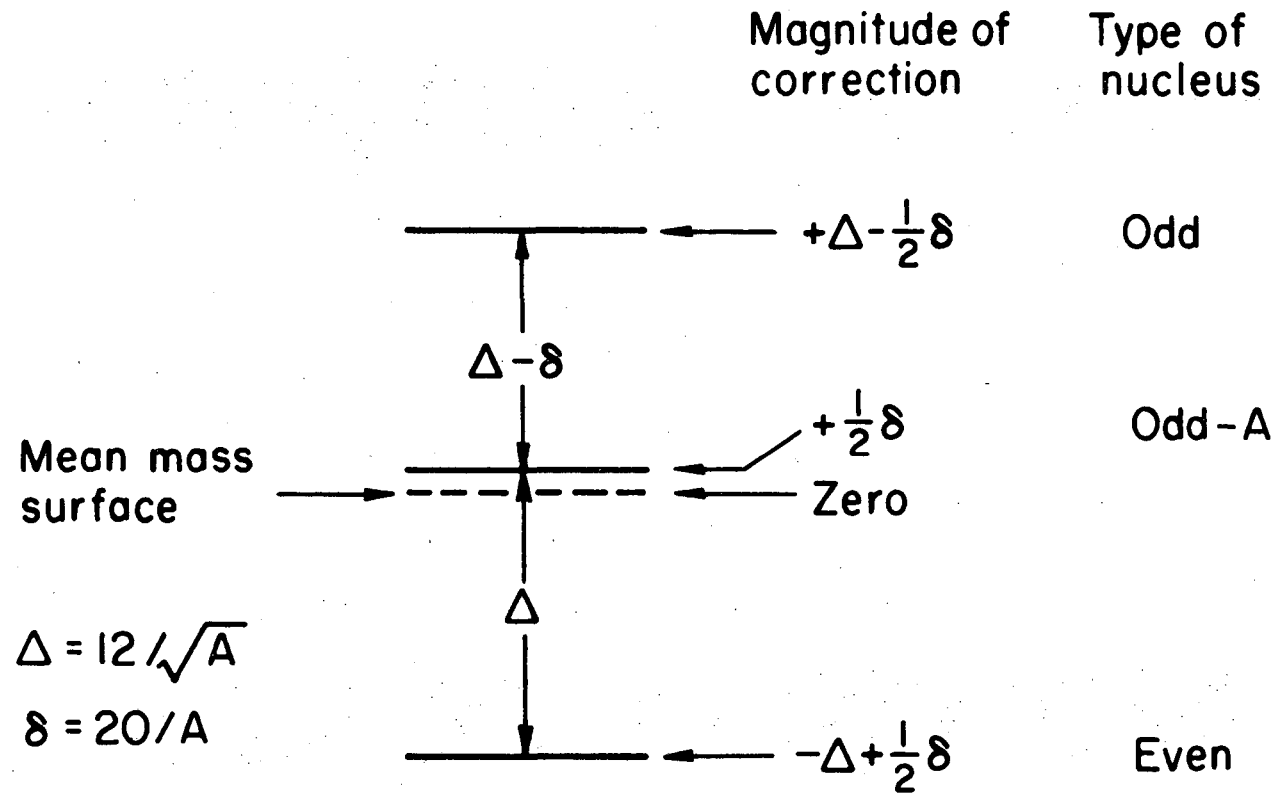
Magnitude of correction
Type of nucleus
$+\Delta-\frac{1}{2}\delta$
Odd
$\Delta-\delta$
$+\frac{1}{2}\delta$
Odd-A
Mean mass surface
Zero
Δ
$\Delta = 12/\sqrt{A}$
$\delta = 20/A$
$-\Delta+\frac{1}{2}\delta$
Even
XBL7412-8331

Fig. 1

No. of particles per orbit	No. of pairs per orbit
1	0
2	1
3	3
4	6

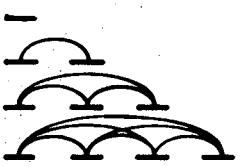

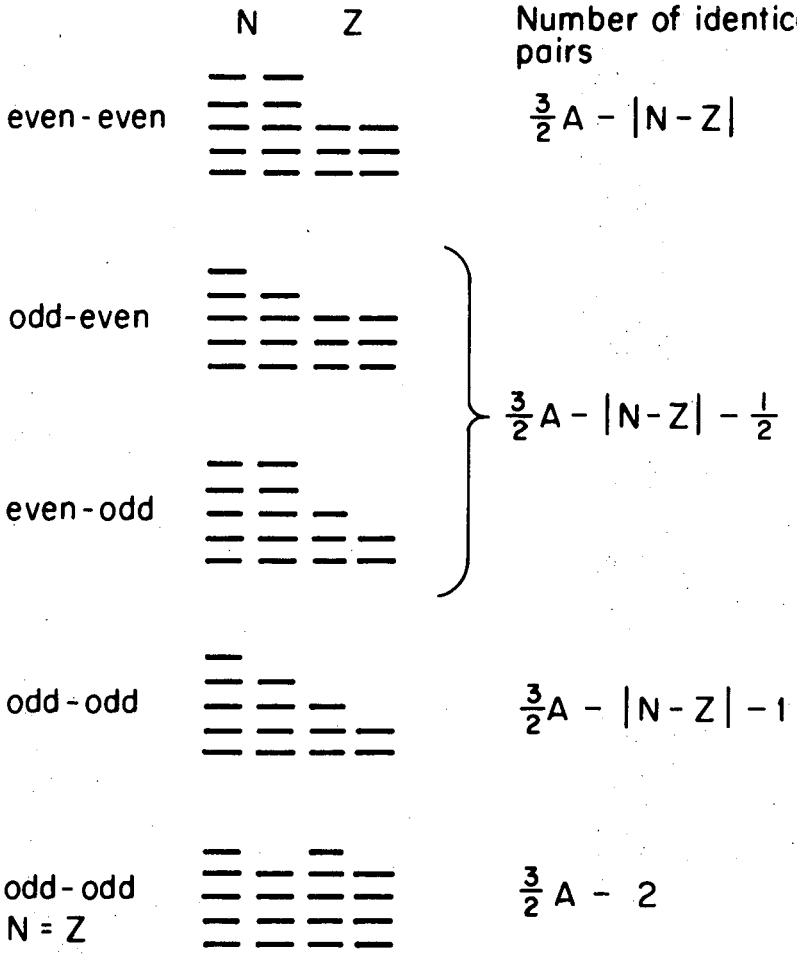

XBL 7412-8334

Fig. 2

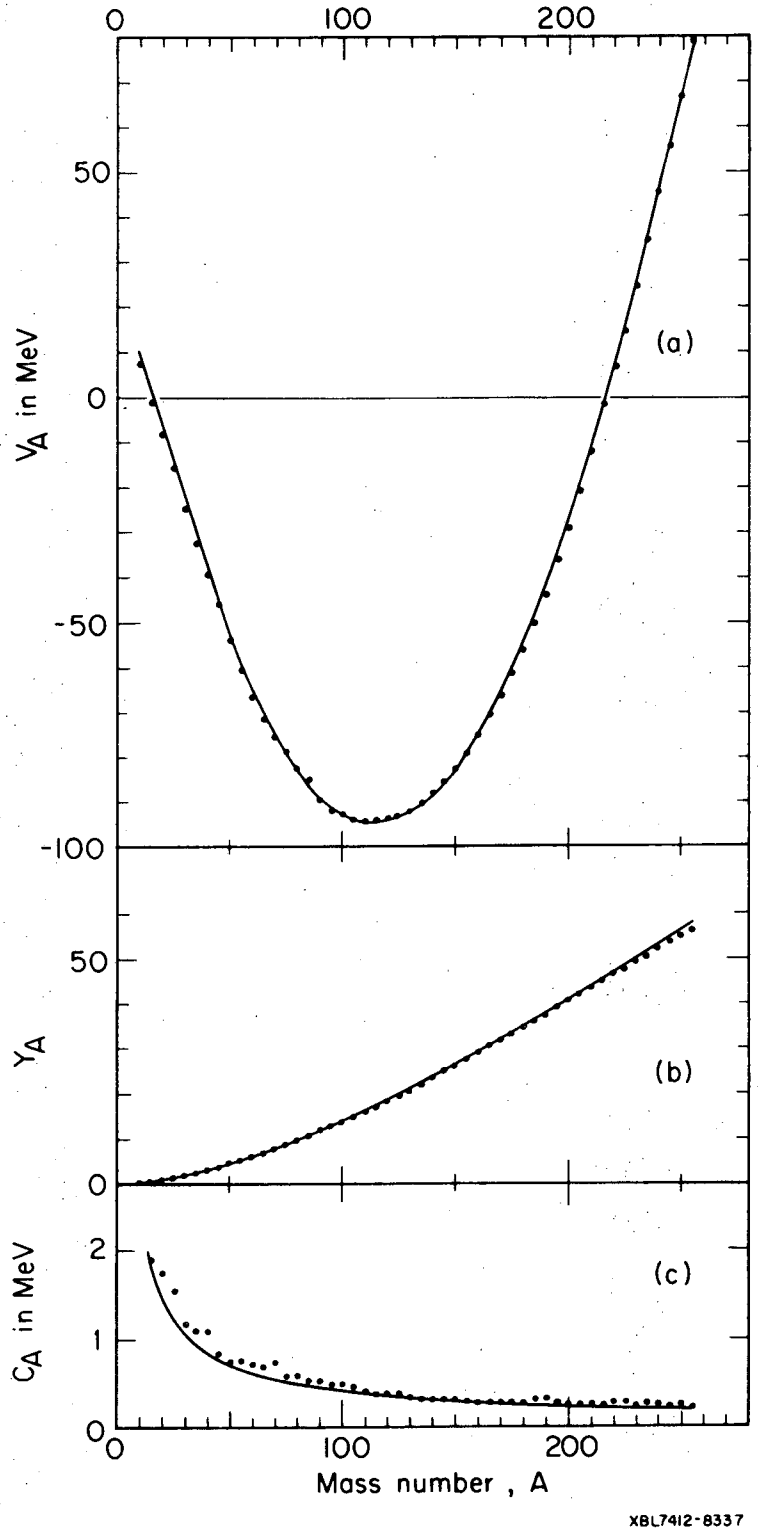
0
100
200
50
0
-50
-100
V_A in MeV
(a)
50
0
Y_A
(b)
2
1
0
C_A in MeV
(c)
0
100
200
Mass number , A
XBL7412-8337

Fig. 3

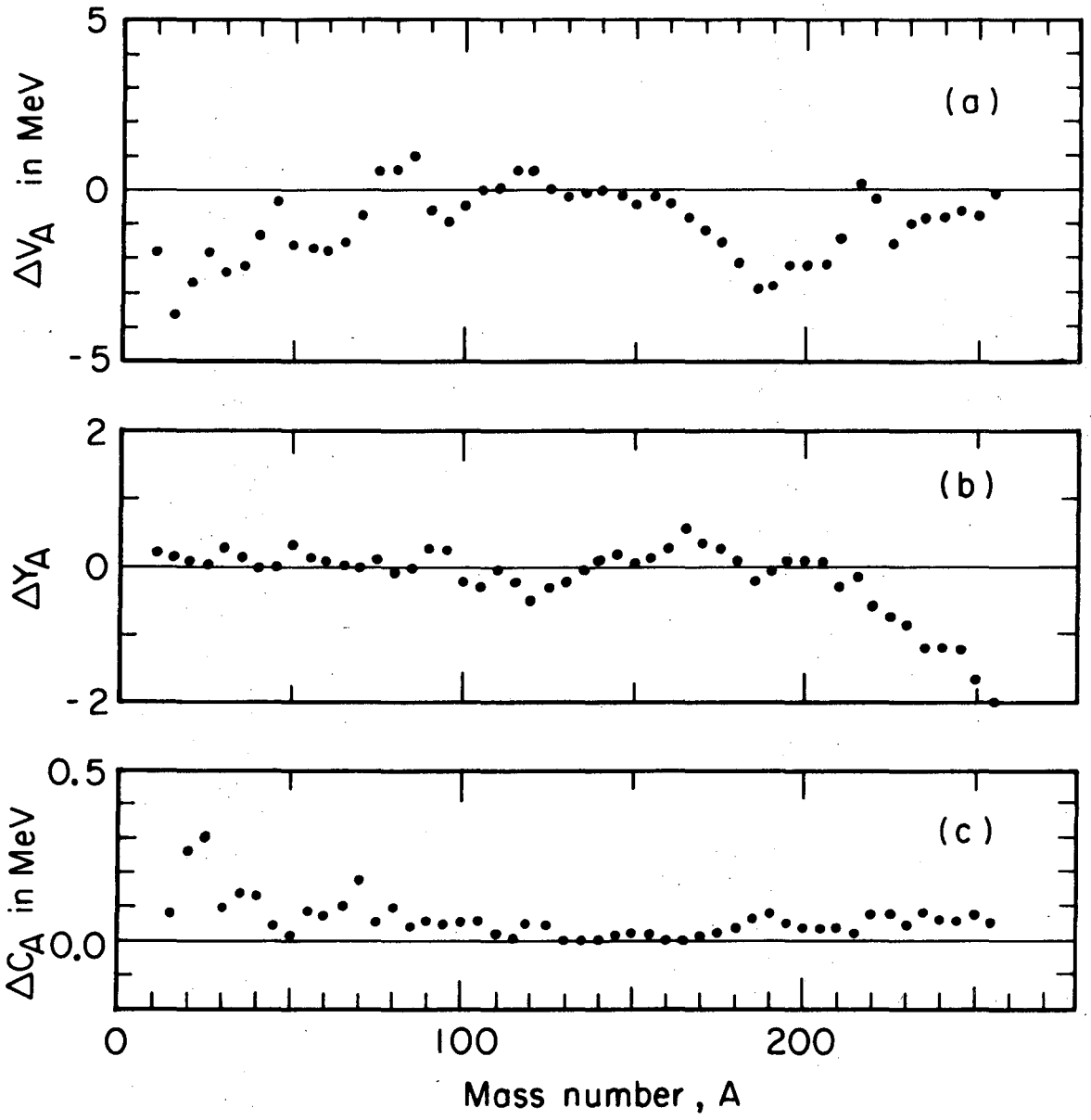
5
0
-5
ΔV_A in MeV
(a)
2
0
-2
ΔY_A
(b)
0.5
0.0
ΔC_A in MeV
(c)
0
100
200
Mass number , A
XBL7412-8336

Fig. 4

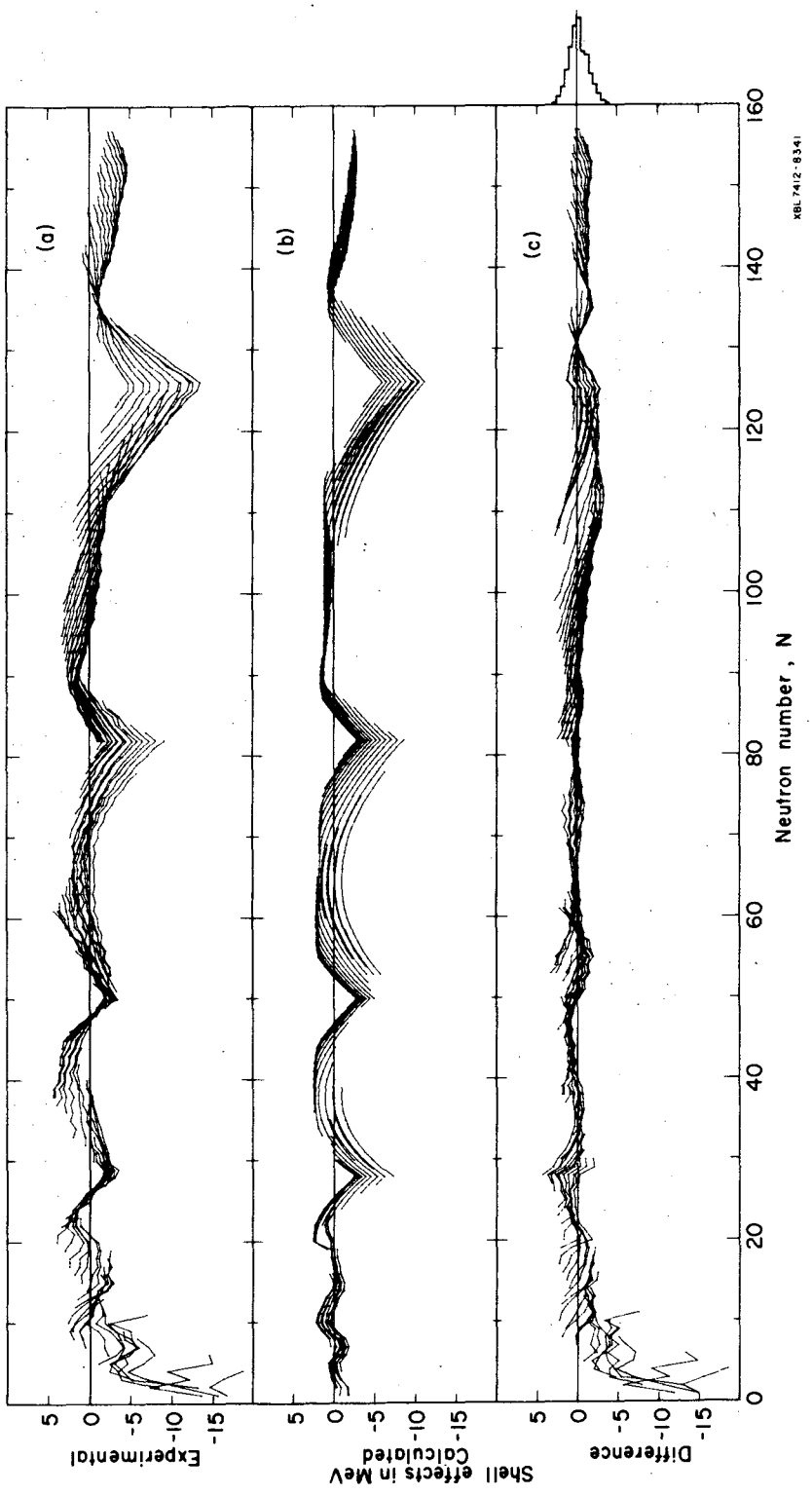
(a)
(b)
(c)
Experimental
Calculated
Difference
Shell effects in MeV
Neutron number, N
5
0
-5
-10
-15
0
20
40
60
80
100
120
140
160
XBL 7412-8341

Fig. 5

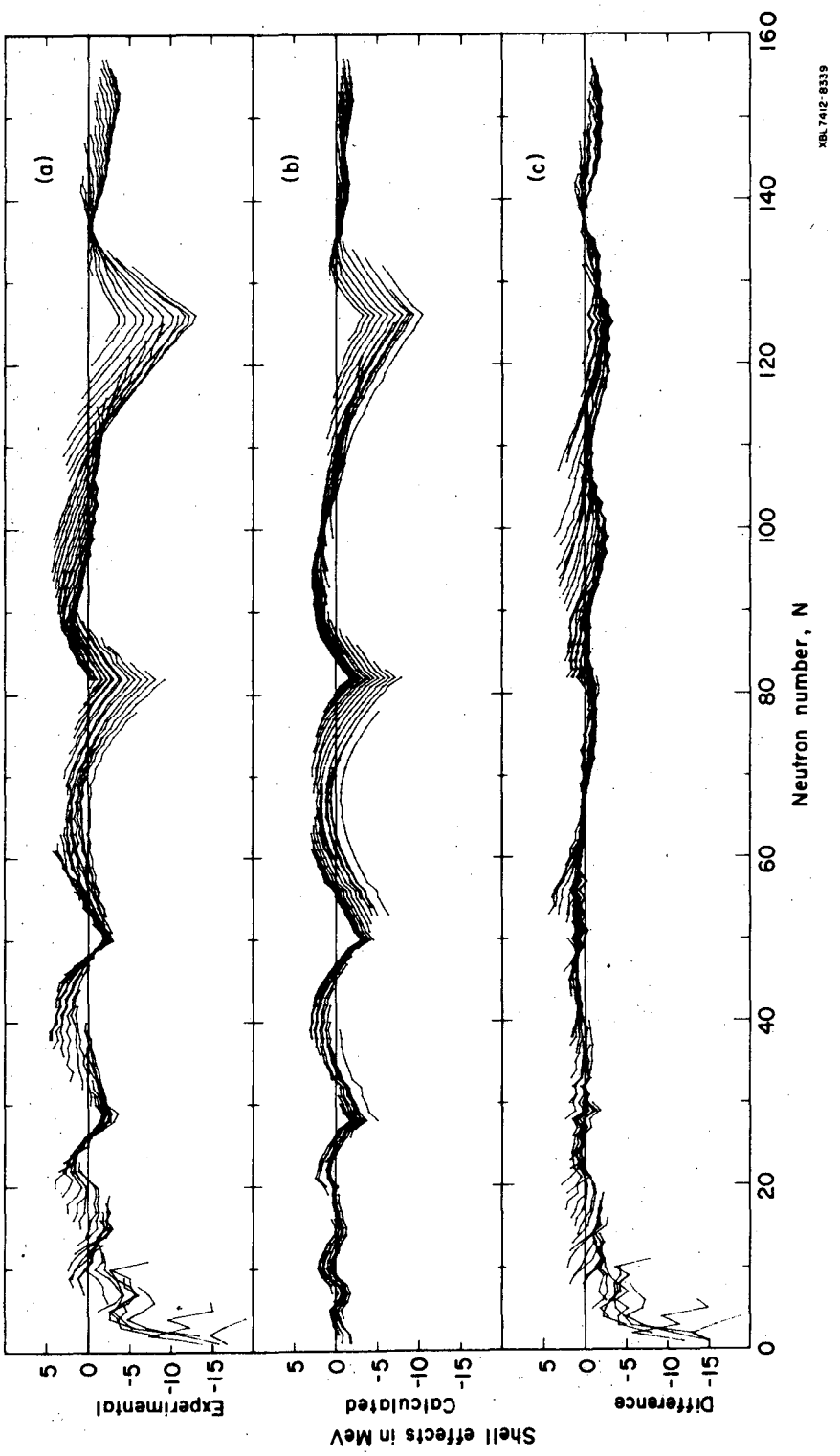
(a)
(b)
(c)
Experimental
Calculated
Difference
Shell effects in MeV
5
0
-5
-10
-15
0
20
40
60
80
100
120
140
160
Neutron number, N
XBL 7412-8339

Fig. 6

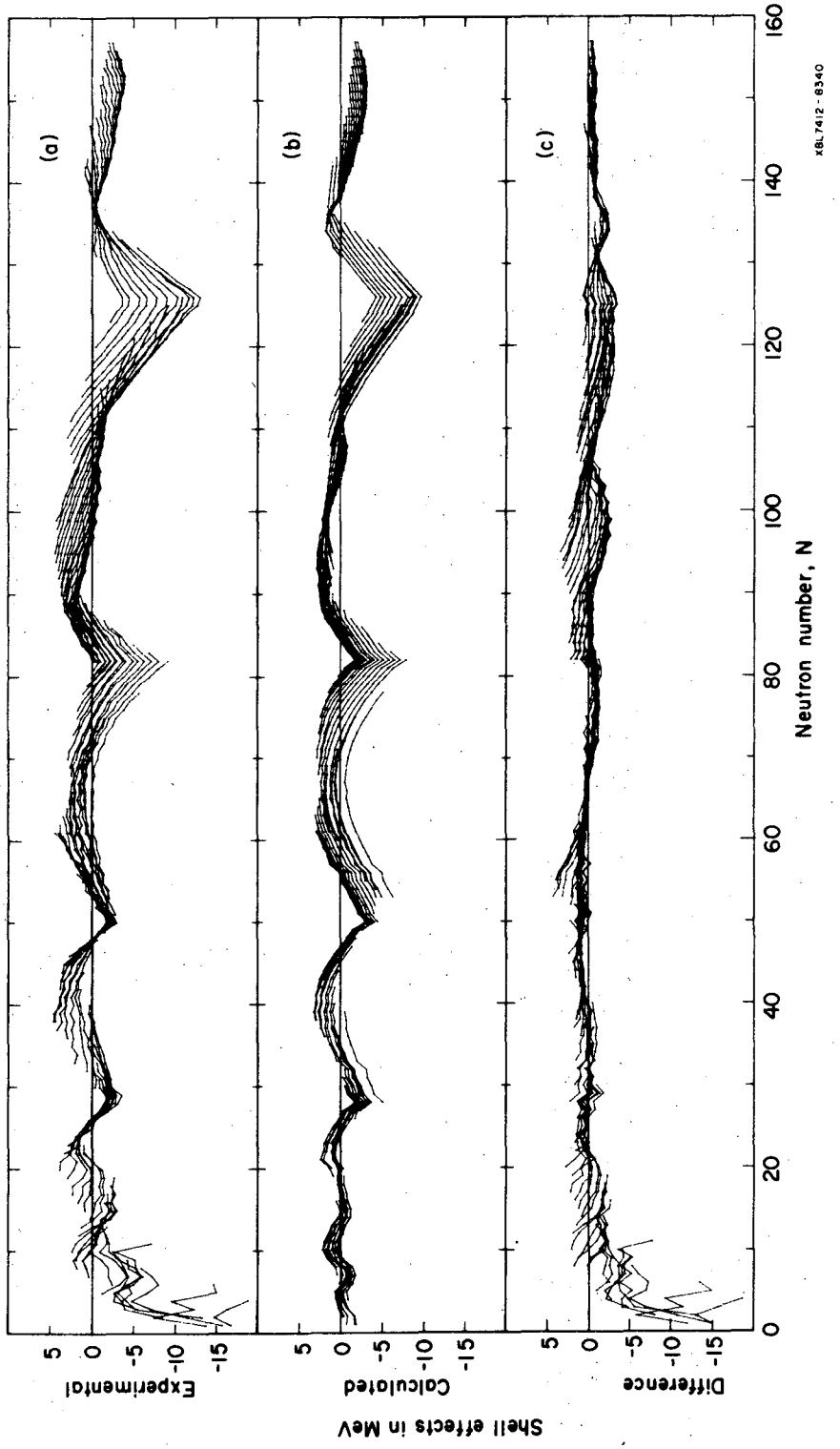
(a)
(b)
(c)
Experimental
Calculated
Difference
Shell effects in MeV
5
0
-5
-10
-15
0
20
40
60
80
100
120
140
160
Neutron number, N
XBL 7412-8340

Fig. 7

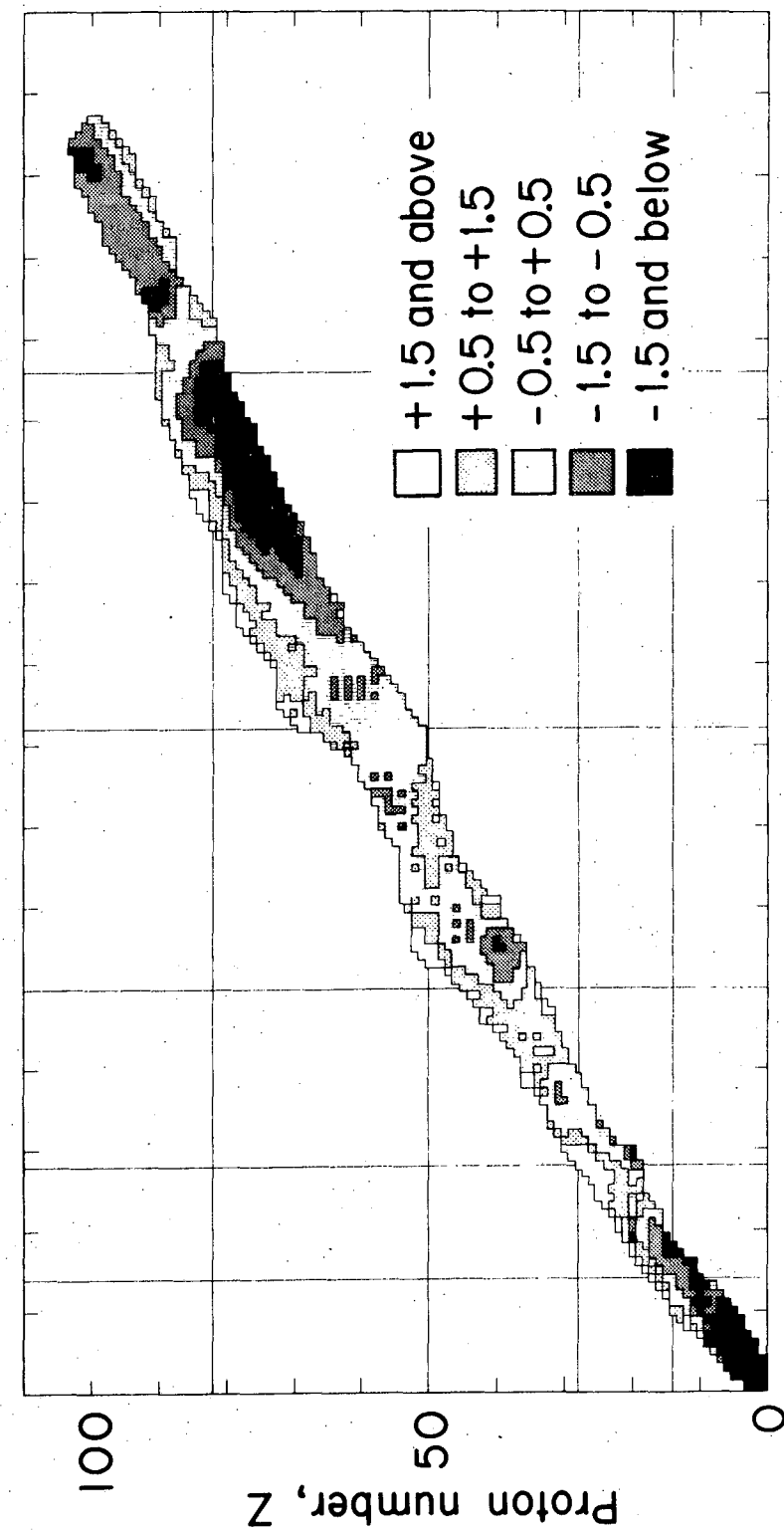
+1.5 and above
+0.5 to +1.5
-0.5 to +0.5
-1.5 to -0.5
-1.5 and below
Neutron number, N
Proton number, Z
0
50
100
150
XBL7410-4346

Fig. 8

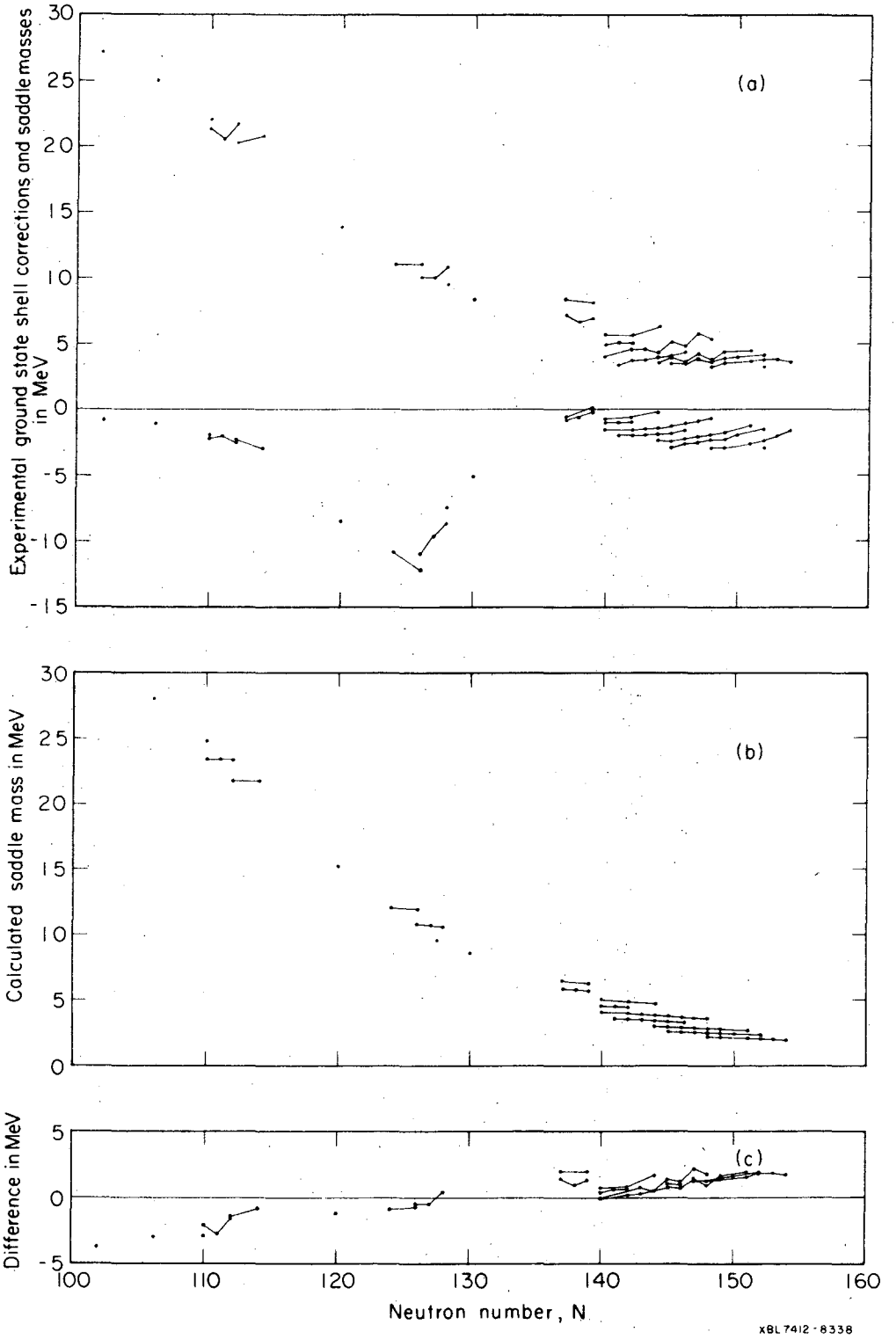
Experimental ground state shell corrections and saddle masses in MeV
(a)
Calculated saddle mass in MeV
(b)
Difference in MeV
(c)
Neutron number, N
XBL 7412-8338

Fig. 9

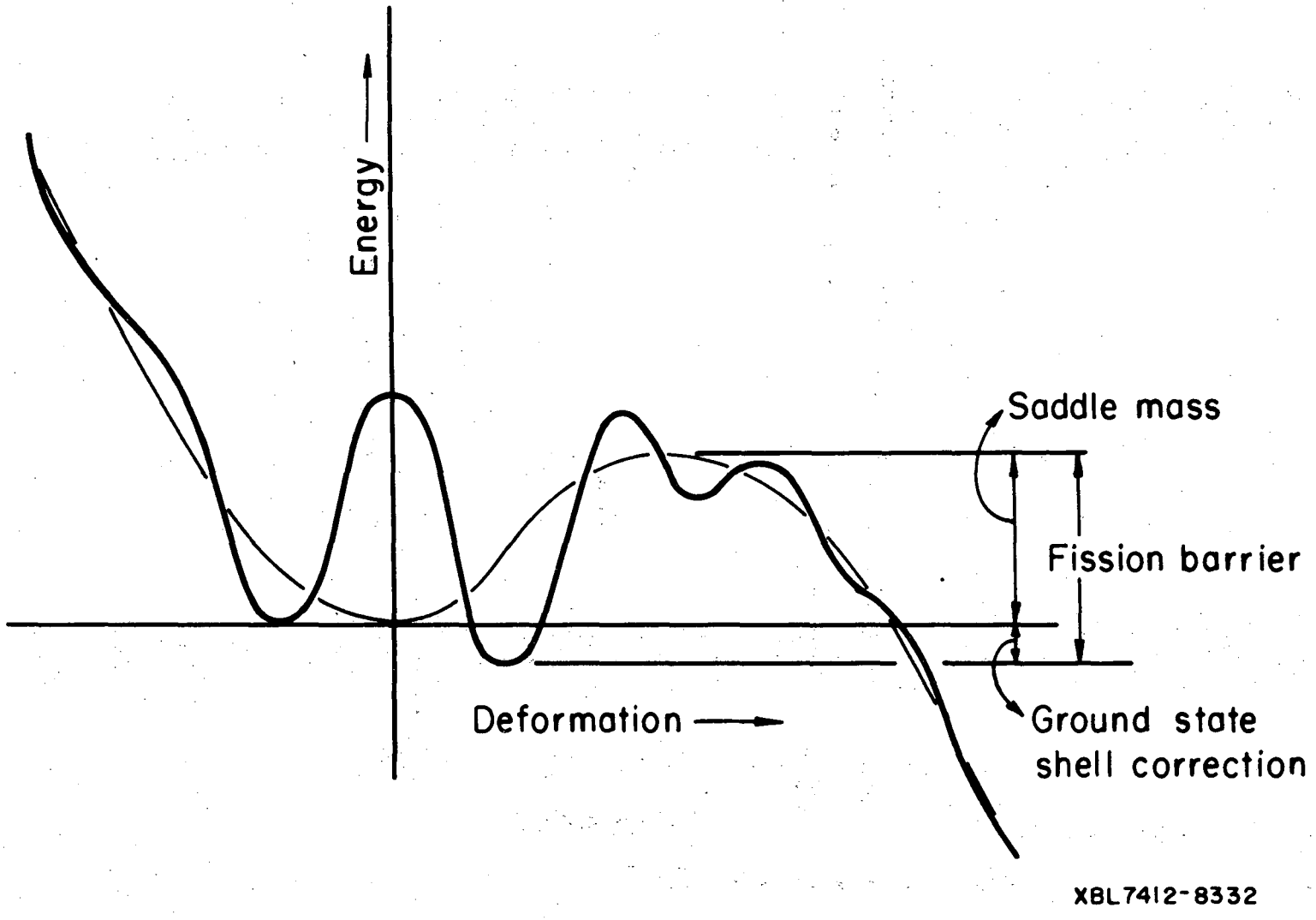
Energy
Saddle mass
Fission barrier
Deformation
Ground state
shell correction
XBL7412-8332

Fig. 10

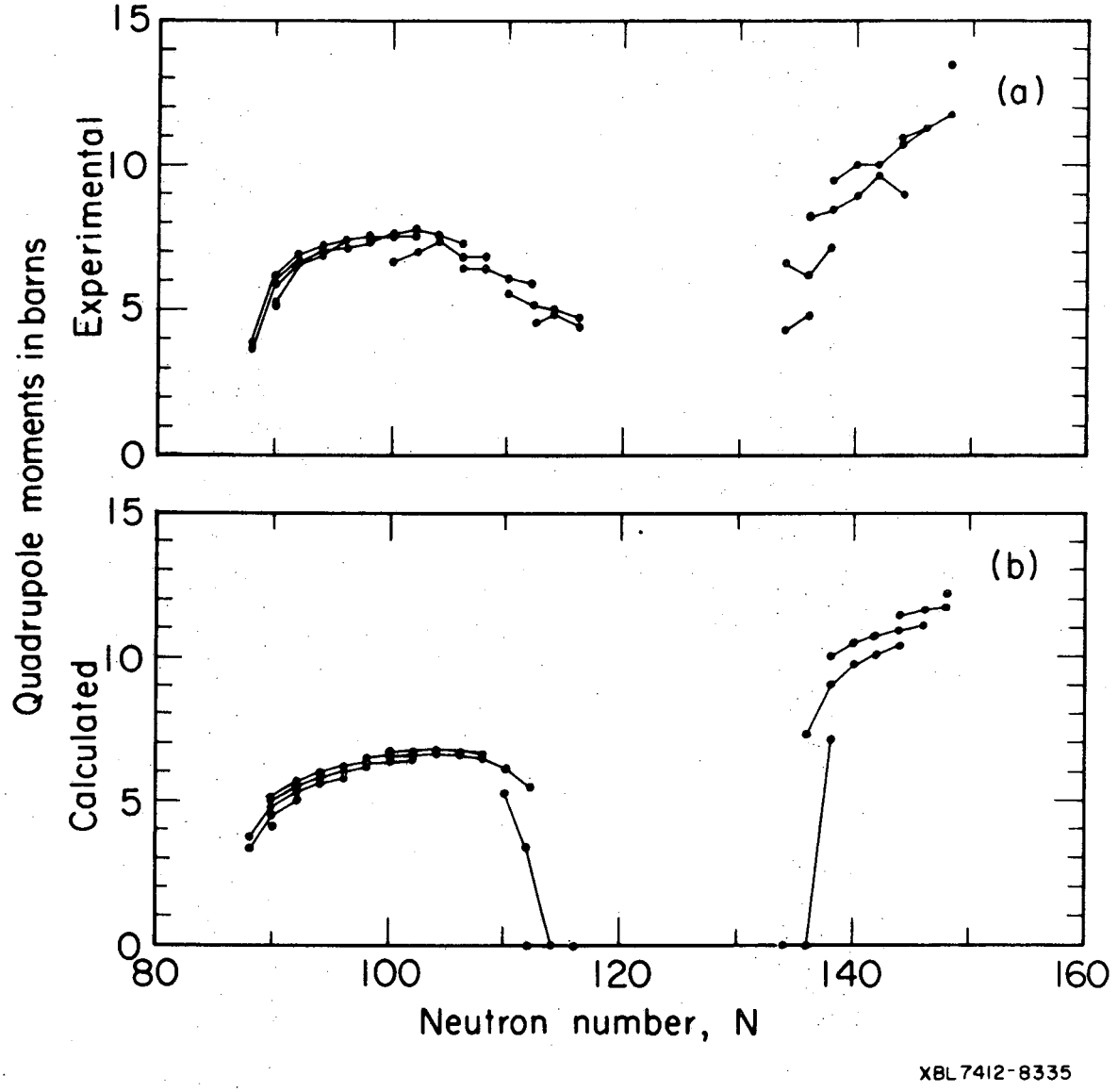
Quadrupole moments in barns
Experimental
Calculated
(a)
(b)
15
10
5
0
80
100
120
140
160
Neutron number, N
XBL 7412-8335

Fig. 11

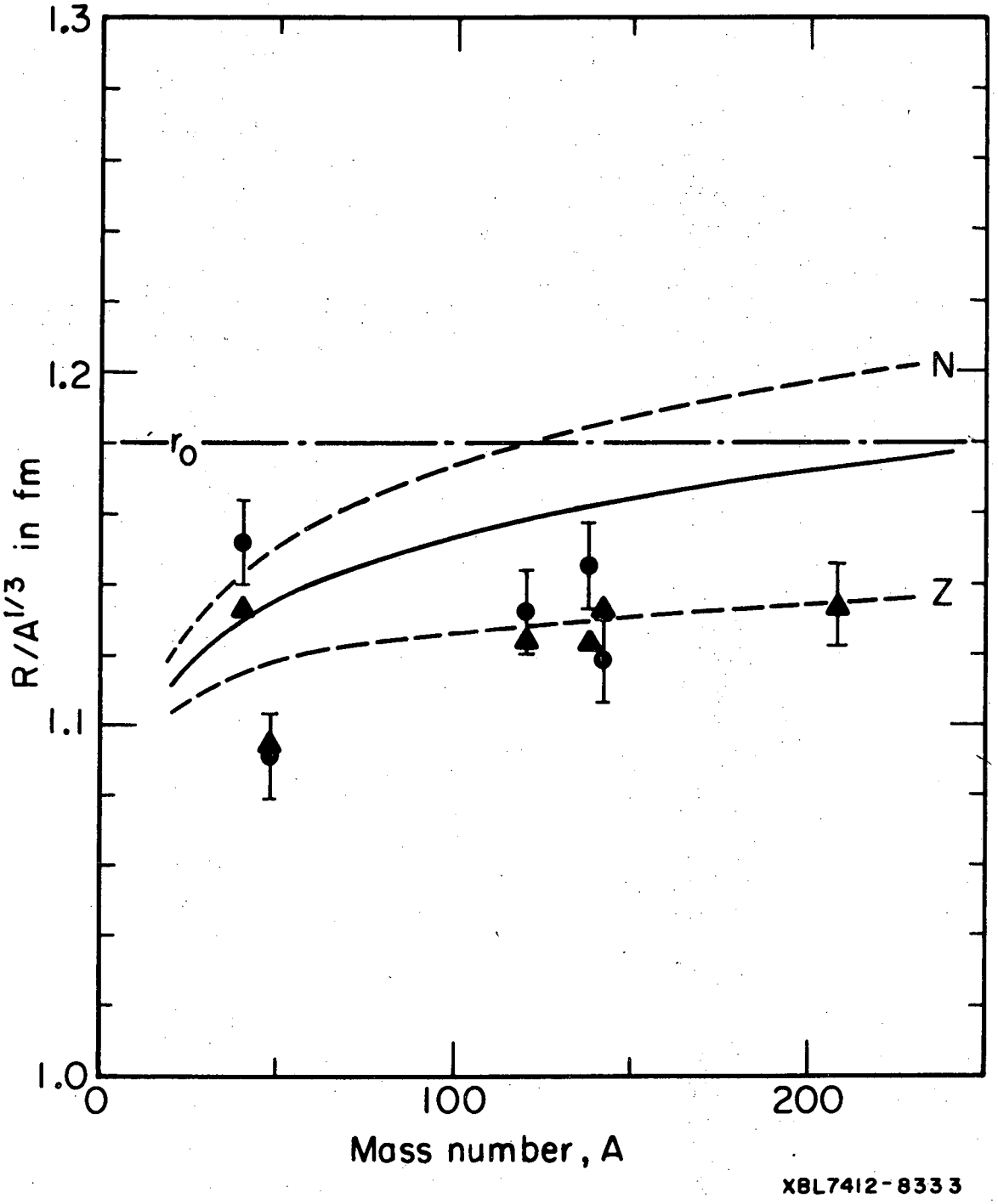

Fig. 12

TECHNICAL INFORMATION DIVISION
LAWRENCE BERKELEY LABORATORY
UNIVERSITY OF CALIFORNIA
BERKELEY, CALIFORNIA 94720